Advances in Nano Research, *Vol. 16, No.6 (2024) 601-613*
https://doi.org/10.12989/anr.2024.16.6.601

Scale-dependent buckling of embedded thermo-electro-magneto-elastic cylindrical nano-shells with different edge conditions

Yifei Gui and Honglei Hu*

School of Mechanical Engineering, Shanghai DianJi University, Shanghai, China

(*Received September 26, 2023, Revised January 23, 2024, Accepted June 5, 2024*)

Abstract. A new analytical buckling solution of a thermo-electro-magneto-elastic (TEME) cylindrical nano-shell made of $BiTiO_3$-$CoFe_2O_4$ materials is obtained based on Hamiltonian approach. The Winkler and Pasternak elastic foundations as well as thermo-electro-magneto-mechanical loadings are applied, and two different types of edge conditions are taken into the investigation. According to nonlocal strain gradient theory (NSGT) and surface elasticity theory in conjunction with the Kirchhoff-Love theory, governing equations of the nano-shell are acquired, and the buckling bifurcation condition is obtained by adopting the Navier's method. The detailed parameter study is conducted to investigate the effects of axial and circumferential wave numbers, scale parameters, elastic foundations, edge conditions and thermo-electro-magnetic loadings on the buckling behavior of the nano-shell. The proposed model can be applied in design and analysis of TEME nano components with multi-field coupled behavior, multiple edge conditions and scale effect.

Keywords: buckling; elastic foundations; TEME cylindrical nano-shell; thermo-electro-magneto-mechanical loadings

1. Introduction

Nanocomposite materials have been applied to laboratory, industrial and commercial applications and also have various applications in industries such as defense, aerospace and automotive. Significant progress has been made in nanocomposite structures by using new groups of TEME nanomaterials, like $BaTiO_3$-$CoFe_2O_4$, is well-proven as prominent materials with numerous potential applications such as actuators and sensors (Fraternali and Paulino 2020, Tiwari *et al*. 2022). The composite TEME nanostructures have received further attention over the previous years for presenting a coupled among the thermal, electric, magnetic and mechanical fields (Moaaz *et al*. 2022, Qu *et al*. 2023, Zhang *et al*. 2020).

To promote the design and manufacture processes, the analysis of the structural stability of TEME nanostructures has drawn a widespread attention recently. The first work is to execute computer simulations and experiments (Frankland *et al*. 2002, Liew *et al*. 2004) to explain small scale effects that affect the behavior of TEME nanostructures, however, it is so sophisticated and needs lots of computing resources. For this reason, to estimate mechanical behavior of structures up to nano scale accurately, the modified and advanced continuum theories accounting length scale and surface effect should be adopted. The NSGT considers the nonlocal stress field also strain gradient stress field, which could depict both stiffness hardening and stiffness softening effects (Lu *et al*. 2019), has been widely used to study nanostructures. Many scholars preferred to choose the NSGT in their attempts to research the scale-dependent mechanical behavior of nano structures (Arefi *et al*. 2020, Dai and Safarpour 2021, Farzad and Parisa 2017, Hosseini *et al*. 2021, Karimi and Farajpour 2019, Momeni-Khabisi and Tahani 2022). Nevertheless, surface effect was not taken into account in their investigation of mechanical behavior using NSGT. Zeighampour *et al*. (2020) investigated the axial buckling of nanotubes regarding the surface effect, and revealed that the surface parameters and surface residual tension have a quite effect on critical load of nanotubes. Recently, the compounding effects of small scale and surface effect on the mechanical behavior of nanostructures have been proceeded by some scholars. Zhang *et al*. (2021) adopted modified couple stress and surface elasticity theories to unify the small size and surface effects. Hamidi *et al*. (2022) discussed the forced torsional vibration of nanobeams with the NSGT in conjunction with surface effect. Presently, researches considering both small size and surface effects mainly focused on nanobeams and nanoplates, while, there is a very limited literature are available for nano-shells (Boyina and Piska 2023, Huang *et al*. 2022, Wang and Jin 2022).

The elastic foundations have capacious applications in engineering such as offshore designing, pipeline network, electromechanical devices and smart material systems (Daikh *et al*. 2021, Jena *et al*. 2019, Pham *et al*. 2023). And the model that considering both normal pressure and transverse shear stress is a generalized depiction of the elastic foundation, is called as Winkler-Pasternak foundation (Ghorbanpour *et al*. 2013, Tran *et al*. 2020, Timesli 2020, 2021). There is limited research have depicted the mechanical characteristics of nanostructures with the elastic foundation using the Winkler-Pasternak model. Li *et al*. (2022) derived analytical solution of the forced vibration of Timoshenko nano-beam under axial tensions supported on Winkler-Pasternak foundation subjected to a harmonic load,

*Corresponding author, Ph.D.,
E-mail: guiyifeiyouxiang@163.com

ISSN: 2287-237X (Print), 2287-2388 (Online)

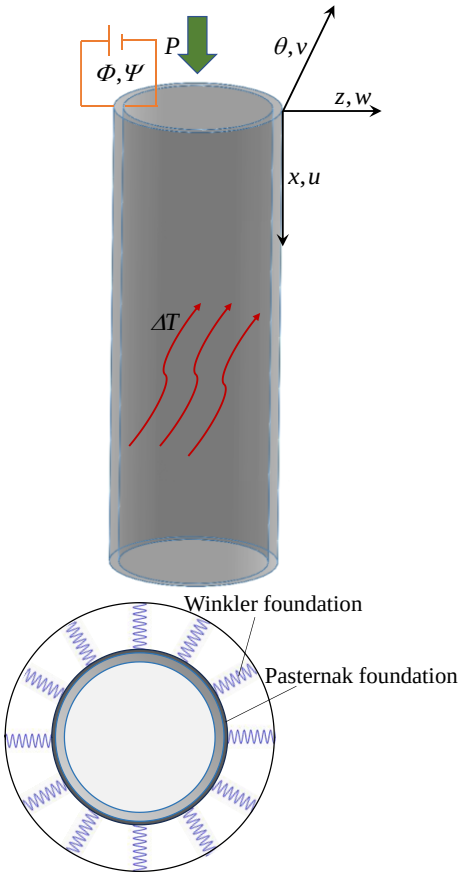

Fig. 1 Configuration and coordinate system of the TEME cylindrical nano-shell on elastic medium

and Timoshenko beam theory and NSGT were employed to describe the nano-beam model. Nicolae *et al*. (2022) investigated on the dynamics of double-walled carbon nanotubes under the influence of Winkler-Pasternak foundation near the primary resonance, and the nonlinear damped and forced vibration was studied using the optimal auxiliary functions method. Mamandi (2023) derived the large deflection of a Euler-Bernoulli cantilever nano-beam on a nonlinear Winkler-Pasternak elastic foundation and under uniformly distributed lateral load using Eringen's nonlocal elasticity theory, considering the nonlinear and linear relationships of curvature-deformation.

There have been many studies on the buckling of composite cylindrical shells (Wang *et al*. 2018a, b, c, Gui and Li 2023, Gui and Wu 2023), according to the authors' knowledge and literature research, the buckling problem of the embedded TEME cylindrical nano-shell under thermo-electro-magneto-mechanical loadings has not been considered before. In the present study, a scale-dependent buckling analysis of an embedded TEME cylindrical nano-shell under thermo-electro-magneto-mechanical loadings is developed for the first time based on Hamiltonian approach. The Winkler and Pasternak elastic foundations are applied to describe the foundation effects, and two different types of edge conditions of the shell are taken into the investigation. According to NSGT and surface elasticity theory in conjunction with the Kirchhoff-Love theory, governing equations are acquired, and the buckling bifurcation condition is obtained by adopting the Navier's method. This new model can account for the nanostructure, thermo-electro-magneto-mechanical coupling and foundation effects.

2. Basic equations for the TEME cylindrical nano-shell

Fig. 1 depicts a TEME cylindrical nano-shell made of $BaTiO_3$-$CoFe_2O_4$ materials resting on a Winkler-Pasternak elastic foundation with length L, mid-surface radius R and thickness h. The coordinate system $(x,\ \theta,\ z)$ is located on the mid-surface of the shell, x -, θ - and z - axes are along the longitudinal, circumferential and radial of the mid-surface, respectively. Winkler and Pasternak coefficients of the elastic foundation are represented by k_w and k_p, respectively. ΔT, $\Phi(x,\theta,z,t)$, $\Psi(x,\theta,z,t)$, P are uniform temperature change, electric potential, magnetic potential and axial load acting on the shell, respectively.

2.1 The scale-dependent TEME cylindrical nano-shell

The strain-displacement relations of the TEME cylindrical nano-shell based on the Kirchhoff-Love theory are given by:

$$\begin{aligned}
\varepsilon_{xx} &= \frac{\partial u}{\partial x} + z\frac{\partial \theta_x}{\partial x} \\
\varepsilon_{\theta\theta} &= \frac{1}{R}\left(\frac{\partial v}{\partial \theta} + w\right) + z\frac{\partial \theta_\theta}{R\partial\theta} \\
\varepsilon_{x\theta} &= \frac{\partial v}{\partial x} + \frac{\partial u}{R\partial\theta} + z\left(\frac{\partial \theta_x}{R\partial\theta} + \frac{\partial \theta_\theta}{\partial x}\right) \\
\varepsilon_{xz} &= \theta_x + \frac{\partial w}{\partial x} \\
\varepsilon_{\theta z} &= \theta_\theta + \frac{\partial w}{R\partial\theta} - \frac{v}{R}
\end{aligned} \tag{1}$$

where, u, v, and w correspond to the displacement components in the x, θ, and z directions, respectively. θ_x and θ_θ are rotational angles between the neutral surface and normal which around the θ and x axes, respectively.

$$\theta_x = -\frac{\partial w}{\partial x},\ \theta_\theta = \frac{v}{R} - \frac{\partial w}{R\partial\theta} \tag{2}$$

The constitutive relations for TEME cylindrical shells polarized along the thickness direction are expressed through relations of stress and strain, which are not taking scale effect into account (Ke *et al*. 2014)

$$\begin{Bmatrix} \sigma_{xx} \\ \sigma_{\theta\theta} \\ \sigma_{x\theta} \\ \sigma_{\theta z} \\ \sigma_{xz} \end{Bmatrix} = \begin{bmatrix} c_{11} & c_{12} & 0 & 0 & 0 \\ c_{12} & c_{22} & 0 & 0 & 0 \\ 0 & 0 & c_{66} & 0 & 0 \\ 0 & 0 & 0 & c_{55} & 0 \\ 0 & 0 & 0 & 0 & c_{44} \end{bmatrix} \cdot \begin{Bmatrix} \varepsilon_{xx} \\ \varepsilon_{\theta\theta} \\ \varepsilon_{x\theta} \\ \varepsilon_{\theta z} \\ \varepsilon_{xz} \end{Bmatrix} - \begin{bmatrix} 0 & 0 & e_{31} \\ 0 & 0 & e_{32} \\ 0 & 0 & 0 \\ 0 & e_{24} & 0 \\ e_{15} & 0 & 0 \end{bmatrix} \cdot \begin{Bmatrix} E_x \\ E_\theta \\ E_z \end{Bmatrix} \tag{3a}$$

$$-\begin{bmatrix}0 & 0 & f_{31}\\ 0 & 0 & f_{32}\\ 0 & 0 & 0\\ 0 & f_{24} & 0\\ f_{15} & 0 & 0\end{bmatrix}\cdot\begin{Bmatrix}H_x\\ H_\theta\\ H_z\end{Bmatrix}-\begin{bmatrix}\beta_{11}\\ \beta_{22}\\ 0\\ 0\\ 0\end{bmatrix}\Delta T$$

$$\begin{Bmatrix}D_x\\ D_\theta\\ D_z\end{Bmatrix}=\begin{bmatrix}0 & 0 & 0 & 0 & e_{15}\\ 0 & 0 & 0 & e_{24} & 0\\ e_{31} & e_{32} & 0 & 0 & 0\end{bmatrix}\cdot\begin{Bmatrix}\varepsilon_{xx}\\ \varepsilon_{\theta\theta}\\ \varepsilon_{x\theta}\\ \varepsilon_{\theta z}\\ \varepsilon_{xz}\end{Bmatrix}+\begin{bmatrix}h_{11} & 0 & 0\\ 0 & h_{22} & 0\\ 0 & 0 & h_{33}\end{bmatrix}\cdot\begin{Bmatrix}E_x\\ E_\theta\\ E_z\end{Bmatrix}+\begin{bmatrix}g_{11} & 0 & 0\\ 0 & g_{22} & 0\\ 0 & 0 & g_{33}\end{bmatrix}\cdot\begin{Bmatrix}H_x\\ H_\theta\\ H_z\end{Bmatrix}+\begin{bmatrix}0\\ 0\\ p_3\end{bmatrix}\Delta T \quad (3b)$$

$$\begin{Bmatrix}B_x\\ B_\theta\\ B_z\end{Bmatrix}=\begin{bmatrix}0 & 0 & 0 & 0 & f_{15}\\ 0 & 0 & 0 & f_{24} & 0\\ f_{31} & f_{32} & 0 & 0 & 0\end{bmatrix}\cdot\begin{Bmatrix}\varepsilon_{xx}\\ \varepsilon_{\theta\theta}\\ \varepsilon_{x\theta}\\ \varepsilon_{\theta z}\\ \varepsilon_{xz}\end{Bmatrix}+\begin{bmatrix}g_{11} & 0 & 0\\ 0 & g_{22} & 0\\ 0 & 0 & g_{33}\end{bmatrix}\cdot\begin{Bmatrix}E_x\\ E_\theta\\ E_z\end{Bmatrix}+\begin{bmatrix}r_{11} & 0 & 0\\ 0 & r_{22} & 0\\ 0 & 0 & r_{33}\end{bmatrix}\cdot\begin{Bmatrix}H_x\\ H_\theta\\ H_z\end{Bmatrix}+\begin{bmatrix}0\\ 0\\ \lambda_3\end{bmatrix}\Delta T \quad (3c)$$

here, σ_{ij}, D_i and B_i denote stress component, electric displacement and magnetic induction, respectively. β_{ij} is thermal modulus. C_{ijkl}, e_{mij}, f_{nij}, h_{im}, g_{in}, p_i, r_{in}, and λ_i represent bulk elastic, piezoelectric, piezomagnetic, dielectric, magnetoelectric, pyroelectric, magnetic, and pyromagnetic constants, respectively. E_m and H_n are the electric field strength and magnetic field strength, respectively, which can be given as

$$E_x=-\frac{\partial\Phi}{\partial x},\ E_\theta=-\frac{1}{R+z}\frac{\partial\Phi}{\partial\theta},\ E_z=-\frac{\partial\Phi}{\partial z} \quad (4a)$$

$$H_x=-\frac{\partial\Psi}{\partial x},\ H_\theta=-\frac{1}{R+z}\frac{\partial\Psi}{\partial\theta},\ H_z=-\frac{\partial\Psi}{\partial z} \quad (4b)$$

The electric and magnetic potentials are defined as a mixture of linear and cosine distributions to clarify the electrically and magnetically influenced behavior of the shell (Jamalpoor *et al*. 2017)

$$\Phi(x,\theta,z,t)=-cos(\eta z)\phi(x,\theta,t)+\frac{2z\phi_0}{h} \quad (5a)$$

$$\Psi(x,\theta,z,t)=-cos(\eta z)\varphi(x,\theta,t)+\frac{2z\varphi_0}{h} \quad (5b)$$

in which, $\eta=\frac{\pi}{h}$. $\phi(x,\theta,t)$ and $\varphi(x,\theta,t)$ represent the electric and magnetic potentials induced by elastic deformation, respectively. φ_0 and ϕ_0 denote initial magnetic and electric potentials, respectively.

Herein, it is significant to consider the surface effect while investigating the buckling of nano-shells. Therefore,

Table 1 Material properties of bulk part and surfaces of $BaTiO_3$-$CoFe_2O_4$ (Karimi and Rafieian 2019, Ni *et al*. 2020, Zur *et al*. 2020)

Elastic (GPa)	$c_{11}=226,\ c_{12}=125,\ c_{13}=124,$ $c_{22}=216,\ c_{23}=124,\ c_{33}=216,$ $c_{44}=44.2,\ c_{55}=44.2,\ c_{66}=50.5$
Piezoelectric (C/m^2)	$e_{31}=-2.2,\ e_{33}=9.3,$ $e_{15}=5.8,\ e_{24}=5.8,\ e_{32}=-2.2$
Dielectric (10^{-9} C^2/Nm^2)	$h_{11}=5.64,\ h_{22}=5.64,\ h_{33}=6.35$
Piezomagnetic (N/Am)	$f_{31}=290.1,\ f_{33}=349.9,$ $f_{15}=275,\ f_{24}=275,\ f_{32}=290.1$
Magnetoelectric (10^{-12} Ns/VC)	$g_{11}=5.367,\ g_{22}=5.367,$ $g_{33}=2737.5$
Magnetic (10^{-6} N s^2 /C^2)	$r_{11}=297,\ r_{22}=297,\ r_{33}=83.5$
Thermal moduli (10^5 N/Km^2)	$\beta_{11}=4.74,\ \beta_{33}=4.53$
Pyroelectric (10^{-6} C /N)	$p_3=25$
Pyromagnetic (10^{-6} N/AmK)	$\lambda_3=5.19$
Surface elastic (N/m)	$c_{11}^s=7.56, c_{22}^s=7.56,$ $c_{12}^s=c_{12}c_{11}^s/c_{11}=4.18,$ $c_{66}^s=(c_{11}^s-c_{12}^s)/2=1.69$
Surface piezoelectric (10^{-8} C/m)	$e_{31}^s=-3,\ e_{32}^s=-3$
Surface piezomagnetic (10^{-8} N/A)	$f_{31}^s=395,\ f_{32}^s=395$

the Gurtin-Murdoch surface elasticity theory is developed to describe the constitutive equations of the TEME cylindrical nano-shell which is made of a bulk part and two surface layers **($z=\pm\frac{h}{2}$)**, to capture the surface influence (Karimi and Rafieian 2019, Ghorbani *et al*. 2020).

$$\begin{bmatrix}\sigma_{xx}^{s\pm}\\ \sigma_{\theta\theta}^{s\pm}\\ \sigma_{x\theta}^{s\pm}\\ \sigma_{\theta z}^{s\pm}\\ \sigma_{xz}^{s\pm}\end{bmatrix}=\begin{bmatrix}c_{11}^s & c_{12}^s & 0 & 0 & 0\\ c_{12}^s & c_{22}^s & 0 & 0 & 0\\ 0 & 0 & c_{66}^s & 0 & 0\\ 0 & 0 & 0 & \tau^s & 0\\ 0 & 0 & 0 & 0 & \tau^s\end{bmatrix}\begin{Bmatrix}\varepsilon_{xx}\\ \varepsilon_{\theta\theta}\\ \varepsilon_{x\theta}\\ \frac{\partial w}{R\partial\theta}\\ \frac{\partial w}{\partial x}\end{Bmatrix}-\begin{bmatrix}0 & 0 & e_{31}^s\\ 0 & 0 & e_{32}^s\\ 0 & 0 & 0\\ 0 & e_{24}^s & 0\\ e_{15}^s & 0 & 0\end{bmatrix}\begin{Bmatrix}E_x\\ E_\theta\\ E_z\end{Bmatrix}-\begin{bmatrix}0 & 0 & f_{31}^s\\ 0 & 0 & f_{32}^s\\ 0 & 0 & 0\\ 0 & f_{24}^s & 0\\ f_{15}^s & 0 & 0\end{bmatrix}\begin{Bmatrix}H_x\\ H_\theta\\ H_z\end{Bmatrix}+\begin{Bmatrix}\tau^s\\ \tau^s\\ 0\\ 0\\ 0\end{Bmatrix},\ z=\pm\frac{h}{2} \quad (6)$$

here, c_{ij}^s, e_{ij}^s and f_{ij}^s denote surface elastic constant, piezoelectric and piezomagnetic constants, respectively. τ^s denotes residual surface stress.

In addition, the NSGT is utilized to describe the scale-dependency of the nano-shells in addition to its smart characteristics, in which the stress consists of nonlocal and

high order stresses to catch the small size effect. Based on the NSGT, the constitutive relations can be stated as

$$(1-(ea)^2\nabla^2)\sigma_{ij} = (1-(l_g)^2\nabla^2)[C_{ijkl}\varepsilon_{kl} - e_{mij}E_m - f_{nij}H_n - \beta_{ij}\Delta T] \quad (7a)$$

$$(1-(ea)^2\nabla^2)D_i = (1-(l_g)^2\nabla^2)[e_{ikl}\varepsilon_{kl} + h_{im}E_m + g_{in}H_n + p_i\Delta T] \quad (7b)$$

$$(1-(ea)^2\nabla^2)B_i = (1-(l_g)^2\nabla^2)[f_{ikl}\varepsilon_{kl} + g_{im}E_m + r_{in}H_n + \lambda_i\Delta T] \quad (7c)$$

$$(1-(ea)^2\nabla^2)\sigma_{ij}^{s\pm} = (1-(l_g)^2\nabla^2)[C_{ijkl}^s\varepsilon_{kl} - e_{mij}^s E_m - f_{nij}^s H_n + \tau_{ij}^s], \quad z=\pm\frac{h}{2} \quad (7d)$$

here, ea represents nonlocal parameter, l_g represents strain gradient parameter. $\nabla^2 = \frac{\partial^2}{\partial x^2} + \frac{\partial^2}{R^2\partial\theta^2}$ refers to the Laplacian operator.

2.2 Hamiltonian description of governing equations

To obtain the governing equations of the TEME cylindrical nano-shell embedded on Winkler and Pasternak foundations, the Hamilton's principle is applied, which can be written as

$$\delta\int_0^t (\Pi_s + \Pi_{s\pm} - \Pi_F - \Pi_T)\,dt = 0 \quad (8)$$

where, Π_s is the strain energy of bulk part, $\Pi_{s\pm}$ are the strain energies of two surfaces:

$$\Pi_s = \frac{1}{2}\int\int\int_V (\sigma_{ij}\varepsilon_{ij} - D_iE_i - B_iH_i)\,Rdzd\theta dx \quad (9)$$

$$\Pi_{s\pm} = \frac{1}{2}\iint_{s+}\sigma_{ij}^{s+}\varepsilon_{ij}ds^+ + \frac{1}{2}\iint_{s-}\sigma_{ij}^{s-}\varepsilon_{ij}ds^- \quad (10)$$

The external work done by elastic foundations can be written in the following form

$$\Pi_T = \frac{1}{2}\int\int_A [k_w w^2 - k_p(\frac{\partial w}{\partial x})^2]\,Rd\theta dx \quad (11)$$

in which, k_w describes the spring element and k_p represents the shear layer.

The shell withstands axial and circumferential forces under temperature change, initial applied electrical load, magnetic load and axial load. The external work Π_F is expressed as

$$\Pi_F = \frac{1}{2}\int\int_A [(N_{Tx}+N_{Ex}+N_{Hx}+P)(\frac{\partial w}{\partial x})^2]\,Rd\theta dx + \frac{1}{2}\int\int_A [\frac{(N_{T\theta}+N_{E\theta}+N_{H\theta})}{R^2}(\frac{\partial w}{\partial\theta})^2]\,Rd\theta dx \quad (12)$$

where, N_{Ex}, N_{Hx}, N_{Tx} are axial electrical, magnetic and thermal loads, respectively. $N_{E\theta}$, $N_{H\theta}$, $N_{T\theta}$ are circumferential electrical, magnetic and thermal loads, respectively.

$$N_{Ex} = N_{E\theta} = -2(e_{31} - \frac{c_{13}e_{33}}{c_{33}})\phi_0$$
$$N_{Hx} = N_{H\theta} = -2(f_{31} - \frac{c_{13}f_{33}}{c_{33}})\varphi_0 \quad (13)$$
$$N_{Tx} = N_{T\theta} = (\beta_{11} - \frac{c_{13}\beta_{33}}{c_{33}})h\Delta T$$

Substituting Eqs. (9)-(12) in Eq. (8), and setting the coefficients of δu, δv, δw, $\delta\phi$, $\delta\varphi$ to zero, produces:

$$\begin{aligned}
&\delta u: \frac{\partial N_{xx}}{\partial x} + \frac{\partial N_{x\theta}}{R\partial\theta} + \frac{\partial\sigma_{xx}^{s+}}{\partial x} + \frac{\partial\sigma_{x\theta}^{s+}}{R\partial\theta} + \frac{\partial\sigma_{xx}^{s-}}{\partial x} + \frac{\partial\sigma_{x\theta}^{s-}}{R\partial\theta} = 0\\
&\delta v: \frac{\partial N_{\theta\theta}}{R\partial\theta} + \frac{\partial N_{x\theta}}{\partial x} + \frac{\partial M_{x\theta}}{R\partial x} + \frac{\partial M_{\theta\theta}}{R^2\partial\theta} + \left(1+\frac{h}{2R}\right)\frac{\partial\sigma_{\theta\theta}^{s+}}{R\partial\theta} + \left(1+\frac{h}{2R}\right)\frac{\partial\sigma_{x\theta}^{s+}}{\partial x} + \left(1-\frac{h}{2R}\right)\frac{\partial\sigma_{\theta\theta}^{s-}}{R\partial\theta} + (1-\frac{h}{2R})\frac{\partial\sigma_{x\theta}^{s-}}{\partial x} = 0\\
&\delta w: \frac{\partial^2 M_{xx}}{\partial x^2} + \frac{2}{R}\frac{\partial^2 M_{x\theta}}{\partial x\partial\theta} + \frac{\partial M^2{}_{\theta\theta}}{R^2\partial\theta^2} - \frac{N_{\theta\theta}}{R} + \left(N_x^0 + P - k_p\right)\frac{\partial^2 w}{\partial x^2} + \frac{N_\theta^0}{R^2}\frac{\partial^2 w}{\partial\theta^2} + k_w w + \frac{h}{2}\frac{\partial^2\sigma_{xx}^{s+}}{\partial x^2} + h\frac{\partial^2\sigma_{x\theta}^{s+}}{R\partial x\partial\theta} + \frac{h}{2}\frac{\partial^2\sigma_{\theta\theta}^{s+}}{R^2\partial\theta^2} - \frac{h}{2}\frac{\partial^2\sigma_{xx}^{s-}}{\partial x^2} - h\frac{\partial^2\sigma_{x\theta}^{s-}}{R\partial x\partial\theta} - \frac{h}{2}\frac{\partial^2\sigma_{\theta\theta}^{s-}}{R^2\partial\theta^2} - \frac{\sigma_{\theta\theta}^{s+}}{R} - \frac{\partial\sigma_{xz}^{s+}}{\partial x} - \frac{\partial\sigma_{\theta z}^{s+}}{R\partial\theta} - \frac{\sigma_{\theta\theta}^{s-}}{R} - \frac{\partial\sigma_{xz}^{s-}}{\partial x} - \frac{\partial\sigma_{\theta z}^{s-}}{R\partial\theta} = 0\\
&\delta\phi: \int_{-\frac{h}{2}}^{\frac{h}{2}} [cos(\eta z)\frac{\partial D_x}{\partial x} + \frac{cos(\eta z)}{R+z}\frac{\partial D_\theta}{\partial\theta} + \eta\, sin(\eta z)D_z]\,dz = 0\\
&\delta\varphi: \int_{-\frac{h}{2}}^{\frac{h}{2}} [cos(\eta z)\frac{\partial B_x}{\partial x} + \frac{cos(\eta z)}{R+z}\frac{\partial B_\theta}{\partial\theta} + \eta\, sin(\eta z)B_z]\,dz = 0
\end{aligned} \quad (14)$$

where, $N_x^0 = N_{Tx} + N_{Ex} + N_{Hx}$, $N_\theta^0 = N_{T\theta} + N_{E\theta} + N_{H\theta}$. The internal force resultants N_{ij} and moment resultants M_{ij} $(i,j = x,\theta)$ can be portrayed by

$$\{N_{xx}, N_{\theta\theta}, N_{x\theta}\} = \int_{-\frac{h}{2}}^{\frac{h}{2}}\{\sigma_{xx}, \sigma_{\theta\theta}, \sigma_{x\theta}\}\,dz$$
$$\{M_{xx}, M_{\theta\theta}, M_{x\theta}\} = \int_{-\frac{h}{2}}^{\frac{h}{2}}\{\sigma_{xx}, \sigma_{\theta\theta}, \sigma_{x\theta}\}\,zdz \quad (15)$$

Based on Eq. (14), integrating Eqs. (7a) - (7d), respectively, and then seeking partial derivatives, produces the following governing equations

$$(c_{11}h + 2c_{11}^s)\frac{\partial^2 u}{\partial x^2} + (c_{66}h + 2c_{66}^s)\frac{\partial^2 u}{R^2\partial\theta^2} + (c_{12}h + c_{66}h + 2c_{12}^s + 2c_{66}^s)\frac{\partial^2 v}{R\partial x\partial\theta} + (c_{12}h + 2c_{12}^s)\frac{\partial w}{R\partial x} = 0 \quad (16a)$$

$$(c_{12}h + c_{66}h + 2c_{12}^s + 2c_{66}^s)\frac{\partial^2 u}{R\partial x\partial\theta} + \left(c_{22}h + \frac{c_{22}h^3}{12R^2} + 2c_{22}^s + \frac{c_{22}^s h^2}{2R^2}\right)\frac{\partial^2 v}{R^2\partial\theta^2} \quad (16b)$$

$$+\left(c_{66}h+\frac{c_{66}h^3}{12R^2}+2c_{66}^s+\frac{c_{66}^s h^2}{2R^2}\right)\frac{\partial^2 v}{\partial x^2}$$
$$+(c_{22}h+2c_{22}^s)\frac{\partial w}{R^2\partial\theta}$$
$$-(\frac{c_{12}h^3}{12}+\frac{c_{66}h^3}{6}+\frac{c_{12}^s h^2}{2}+c_{66}^s h^2)\frac{\partial^3 w}{R^2\partial x^2\partial\theta}$$
$$-(\frac{c_{22}h^3}{12}+\frac{c_{22}^s h^2}{2})\frac{\partial^3 w}{R^4\partial\theta^3}$$
$$+(\frac{\tilde{e}_{32}}{R^2}+\frac{he_{32}^s}{R^2}\eta)\frac{\partial\phi}{\partial\theta}+(\frac{\tilde{f}_{32}}{R^2}+\frac{hf_{32}^s}{R^2}\eta)\frac{\partial\varphi}{\partial\theta}=0$$

$$-\left(\frac{c_{11}h^3}{12}+\frac{c_{11}^s h^2}{2}\right)\frac{\partial^4 w}{\partial x^4}$$
$$-\left(\frac{c_{12}h^3}{6}+\frac{c_{66}h^3}{3}+c_{12}^s h^2+2c_{66}^s h^2\right)\frac{\partial^4 w}{R^2\partial x^2\partial\theta^2}$$
$$-\left(\frac{c_{22}h^3}{12}+\frac{c_{22}^s h^2}{2}\right)\frac{\partial^4 w}{R^4\partial\theta^4}$$
$$+(\tilde{e}_{31}+e_{31}^s h\eta)\frac{\partial^2\phi}{\partial x^2}+\left(\tilde{f}_{31}+f_{31}^s h\eta\right)\frac{\partial^2\varphi}{\partial x^2}$$
$$+(\tilde{e}_{32}+e_{32}^s h\eta)\frac{\partial^2\phi}{R^2\partial\theta^2}+\left(\tilde{f}_{32}+f_{32}^s h\eta\right)\frac{\partial^2\varphi}{R^2\partial\theta^2}$$
$$+\left(\frac{c_{12}h^3}{12}+\frac{c_{66}h^3}{6}+\frac{c_{12}^s h^2}{2}+c_{66}^s h^2\right)\frac{\partial^3 v}{R^2\partial x^2\partial\theta}$$
$$+\left(\frac{c_{22}h^3}{12}+\frac{c_{22}^s h^2}{2}\right)\frac{\partial^3 v}{R^4\partial\theta^3}-(c_{12}h+2c_{12}^s)\frac{\partial u}{R\partial x}$$
$$-(c_{22}h+2c_{22}^s)(\frac{\partial v}{R^2\partial\theta}+\frac{w}{R^2})-2\tau^s\frac{\partial^2 w}{\partial x^2}$$
$$-2\tau^s\frac{\partial^2 w}{R^2\partial\theta^2}+(1-(ea)^2\nabla^2)[(N_x^0+P-k_p)\frac{\partial^2 w}{\partial x^2}$$
$$+\frac{N_\theta^0}{R^2}\frac{\partial^2 w}{\partial\theta^2}+k_w w]=0 \qquad (16c)$$

$$(1-l_g^2\nabla^2)(\tilde{h}_{11}\frac{\partial^2\phi}{\partial x^2}+\tilde{g}_{11}\frac{\partial^2\varphi}{\partial x^2}+\tilde{h}_{22}\frac{\partial^2\phi}{\partial\theta^2}+\tilde{g}_{22}\frac{\partial^2\varphi}{\partial\theta^2})$$
$$+(1-(ea)^2\nabla^2)[\tilde{e}_{31}\frac{\partial^2 w}{\partial x^2}+\frac{\tilde{e}_{32}}{R^2}(\frac{\partial^2 w}{\partial\theta^2}-\frac{\partial v}{\partial\theta})$$
$$+\tilde{h}_{33}\phi+\tilde{g}_{33}\varphi]=0 \qquad (16d)$$

$$(1-l_g^2\nabla^2)(\tilde{g}_{11}\frac{\partial^2\phi}{\partial x^2}+\tilde{r}_{11}\frac{\partial^2\varphi}{\partial x^2}+\tilde{g}_{22}\frac{\partial^2\phi}{\partial\theta^2}+\tilde{r}_{22}\frac{\partial^2\varphi}{\partial\theta^2})$$
$$+(1-(ea)^2\nabla^2)[\tilde{f}_{31}\frac{\partial^2 w}{\partial x^2}+\frac{\tilde{f}_{32}}{R^2}(\frac{\partial^2 w}{\partial\theta^2}-\frac{\partial v}{\partial\theta})$$
$$+\tilde{g}_{33}\phi+\tilde{r}_{33}\varphi]=0 \qquad (16e)$$

where,

$$\tilde{e}_{31}=\int_{-\frac{h}{2}}^{\frac{h}{2}}e_{31}\,\eta\,sin(\eta z)zdz,\qquad \tilde{f}_{31}=\int_{-\frac{h}{2}}^{\frac{h}{2}}f_{31}\,\eta\,sin(\eta z)zdz,$$
$$\tilde{e}_{32}=\int_{-\frac{h}{2}}^{\frac{h}{2}}e_{32}\,\eta\,sin(\eta z)zdz,\qquad \tilde{f}_{32}=\int_{-\frac{h}{2}}^{\frac{h}{2}}f_{32}\,\eta\,sin(\eta z)zdz,$$
$$\tilde{h}_{11}=\int_{-\frac{h}{2}}^{\frac{h}{2}}h_{11}\,cos^2(\eta z)dz,\qquad \tilde{g}_{11}=\int_{-\frac{h}{2}}^{\frac{h}{2}}g_{11}\,cos^2(\eta z)dz,$$
$$\tilde{h}_{22}=\int_{-\frac{h}{2}}^{\frac{h}{2}}h_{22}\left(\frac{cos(\eta z)}{R+z}\right)^2dz,\qquad \tilde{g}_{22}=\int_{-\frac{h}{2}}^{\frac{h}{2}}g_{22}\left(\frac{cos(\eta z)}{R+z}\right)^2dz,$$
$$\tilde{h}_{33}=\int_{-\frac{h}{2}}^{\frac{h}{2}}h_{33}\,[\eta\,sin(\eta z)]^2dz,\qquad \tilde{g}_{33}=\int_{-\frac{h}{2}}^{\frac{h}{2}}g_{33}\,[\eta\,sin(\eta z)]^2dz,$$
$$\tilde{r}_{11}=\int_{-\frac{h}{2}}^{\frac{h}{2}}r_{11}\,cos^2(\eta z)dz,\qquad \tilde{r}_{22}=\int_{-\frac{h}{2}}^{\frac{h}{2}}r_{22}\left(\frac{cos(\eta z)}{R+z}\right)^2dz,$$
$$\tilde{r}_{33}=\int_{-\frac{h}{2}}^{\frac{h}{2}}r_{33}\,[\eta\,sin(\eta z)]^2dz$$

3. Buckling process for different edge conditions

In this part, introducing the Navier's solution to establish the displacements for the TEME cylindrical nano-shell with simply-supported (S-S) and clamped-clamped (C-C) edge conditions, respectively. And the electric and magnetic potentials at the edges are considered to be zero.

3.1 TEME cylindrical nano-shells with S-S edges

The associated edge conditions are

$$\frac{\partial u}{\partial x}=v=w=\frac{\partial^2 w}{\partial x^2}=\phi=\varphi=0,\quad (x=0,L) \qquad (17)$$

The displacement fields of the shell with S-S edges can be defined as

$$\begin{aligned}u(x,\theta,t)&=U_{mn}^s\,cos(\lambda_m x)\,cos(n\theta)\\ v(x,\theta,t)&=V_{mn}^s\,sin(\lambda_m x)\,sin(n\theta)\\ w(x,\theta,t)&=W_{mn}^s\,sin(\lambda_m x)\,cos(n\theta)\\ \phi(x,\theta,t)&=\phi_{mn}^s\,sin(\lambda_m x)\,cos(n\theta)\\ \varphi(x,\theta,t)&=\varphi_{mn}^s\,sin(\lambda_m x)\,cos(n\theta)\end{aligned} \qquad (18)$$

here, $\lambda_m=\frac{m\pi}{L}$. U_{mn}^s, V_{mn}^s, W_{mn}^s, ϕ_{mn}^s, φ_{mn}^s denote time-dependent unknown coefficients. m and n are axial and circumferential wave numbers, respectively.

Substituting Eq. (18) into Eq. (16), produces

$$\begin{bmatrix}k_{11}^s & k_{12}^s & k_{13}^s & k_{14}^s & k_{15}^s\\ k_{21}^s & k_{22}^s & k_{23}^s & k_{24}^s & k_{25}^s\\ k_{31}^s & k_{32}^s & k_{33}^s & k_{34}^s & k_{35}^s\\ k_{41}^s & k_{42}^s & k_{43}^s & k_{44}^s & k_{45}^s\\ k_{51}^s & k_{52}^s & k_{53}^s & k_{54}^s & k_{55}^s\end{bmatrix}\cdot\begin{bmatrix}U_{mn}^s\\ V_{mn}^s\\ W_{mn}^s\\ \phi_{mn}^s\\ \varphi_{mn}^s\end{bmatrix}=\mathbf{0} \qquad (19)$$

where

$$k_{11}^s=-(c_{11}h+2c_{11}^s)\lambda_m^2-(c_{66}h+2c_{66}^s)\frac{n^2}{R^2}$$
$$k_{12}^s=k_{21}^s=(c_{12}h+c_{66}h+2c_{12}^s+2c_{66}^s)\frac{n\lambda_m}{R}$$
$$k_{13}^s=k_{31}^s=(c_{12}h+2c_{12}^s)\frac{\lambda_m}{R}$$
$$k_{14}^s=k_{41}^s=k_{15}^s=k_{51}^s=0$$
$$k_{22}^s=-(c_{22}h+2c_{22}^s+\frac{c_{22}h^3+6h^2c_{22}^s}{12R^2})\frac{n^2}{R^2}$$
$$-(c_{66}h+\frac{c_{66}h^3}{12R^2}+2c_{66}^s+\frac{h^2c_{66}^s}{2R^2})\lambda_m^2$$
$$k_{23}^s=k_{32}^s=-(c_{22}h+2c_{22}^s)\frac{n}{R^2}$$
$$-(\frac{c_{12}h}{12}+\frac{c_{66}h}{6}+\frac{c_{12}^s}{2}+c_{66}^s)\frac{h^2n\lambda_m^2}{R^2}-(\frac{c_{22}h}{6}+c_{22}^s)\frac{h^2n^3}{2R^4}$$
$$k_{24}^s=-(\tilde{e}_{32}+e_{32}^s h\eta)\frac{n}{R^2}$$
$$k_{25}^s=-(\tilde{f}_{32}+f_{32}^s h\eta)\frac{n}{R^2}$$
$$k_{33}^s=-[\frac{c_{11}}{12}h^3+\frac{c_{11}^s}{2}h^2+(ea)^2(N_x^0+P-k_p)]\lambda_m^4$$

$$-[\frac{c_{12}}{6}h^3+\frac{c_{66}}{3}h^3+c_{12}^s h^2+2c_{66}^s h^2$$
$$+(ea)^2(N_x^0+P-k_p)+(ea)^2N_\theta^0]\frac{\lambda_m^2 n^2}{R^2}$$
$$-[\frac{c_{22}}{12}h^3+\frac{c_{22}^s}{2}h^2+(ea)^2N_\theta^0]\frac{n^4}{R^4}-(c_{22}h+2c_{22}^s)\frac{1}{R^2}$$
$$+k_w+[2\tau^s-(N_x^0+P-k_p)$$
$$+(ea)^2k_w]\lambda_m^2+[2\tau^s-N_\theta^0+(ea)^2k_w]\frac{n^2}{R^2}$$
$$k_{34}^s=-(\tilde{e}_{31}+e_{31}^s h\eta)\lambda_m^2-(\tilde{e}_{32}+e_{32}^s h\eta)\frac{n^2}{R^2}$$
$$k_{35}^s=-(\tilde{f}_{31}+f_{31}^s h\eta)\lambda_m^2-(\tilde{f}_{32}+f_{32}^s h\eta)\frac{n^2}{R^2}$$
$$k_{42}^s=\frac{n\tilde{e}_{32}}{R^2}[1+(ea)^2\lambda_m^2+(ea)^2\frac{n^2}{R^2}]$$
$$k_{43}^s=\tilde{e}_{31}\lambda_m^2[1+(ea)^2\lambda_m^2]+\frac{\tilde{e}_{32}}{R^2}n^2$$
$$+\frac{(ea)^2}{R^2}(\tilde{e}_{31}+\tilde{e}_{32})n^2\lambda_m^2+(ea)^2\frac{\tilde{e}_{32}}{R^4}n^4$$
$$k_{44}^s=-\tilde{h}_{11}\lambda_m^2-\tilde{h}_{22}n^2$$
$$-l_g^2[\tilde{h}_{11}\lambda_m^4+(\frac{\tilde{h}_{11}}{R^2}+\tilde{h}_{22})n^2\lambda_m^2+\frac{\tilde{h}_{22}}{R^2}n^4]$$
$$-\tilde{h}_{33}[1+(ea)^2\lambda_m^2+(ea)^2\frac{n^2}{R^2}]$$
$$k_{45}^s=-\tilde{g}_{11}\lambda_m^2-\tilde{g}_{22}n^2$$
$$-l_g^2[\tilde{g}_{11}\lambda_m^4+(\frac{\tilde{g}_{11}}{R^2}+\tilde{g}_{22})n^2\lambda_m^2+\frac{\tilde{g}_{22}}{R^2}n^4]$$
$$-\tilde{g}_{33}[1+(ea)^2\lambda_m^2+(ea)^2\frac{n^2}{R^2}]$$
$$k_{52}^s=\frac{n\tilde{f}_{32}}{R^2}[1+(ea)^2\lambda_m^2+(ea)^2\frac{n^2}{R^2}]$$
$$k_{53}^s=\tilde{f}_{31}\lambda_m^2[1+(ea)^2\lambda_m^2]+\frac{\tilde{f}_{32}}{R^2}n^2$$
$$+\frac{(ea)^2}{R^2}(\tilde{f}_{31}+\tilde{f}_{32})n^2\lambda_m^2+(ea)^2\frac{\tilde{f}_{32}}{R^4}n^4$$
$$k_{54}^s=-\tilde{g}_{11}\lambda_m^2-\tilde{g}_{22}n^2$$
$$-l_g^2[\tilde{g}_{11}\lambda_m^4+(\frac{\tilde{g}_{11}}{R^2}+\tilde{g}_{22})n^2\lambda_m^2+\frac{\tilde{g}_{22}}{R^2}n^4]$$
$$-\tilde{g}_{33}[1+(ea)^2\lambda_m^2+(ea)^2\frac{n^2}{R^2}]$$
$$k_{55}^s=-\tilde{r}_{11}\lambda_m^2-\tilde{r}_{22}n^2$$
$$-l_g^2[\tilde{r}_{11}\lambda_m^4+(\frac{\tilde{r}_{11}}{R^2}+\tilde{r}_{22})n^2\lambda_m^2+\frac{\tilde{r}_{22}}{R^2}n^4]$$
$$-\tilde{r}_{33}[1+(ea)^2\lambda_m^2+(ea)^2\frac{n^2}{R^2}]$$

To obtain non-trivial solutions, the determinant of the coefficient matrix in Eq. (19) should be vanished. In other words, the bifurcation condition of the buckling process is attained by setting the determinant to zero.

3.2 TEME cylindrical nano-shells with C-C edges

Similarly, the associated edge conditions are

$$u=v=w=\frac{\partial w}{\partial\theta}=\phi=\varphi=0,\quad (x=0,L) \tag{20}$$

In this case, the displacement fields can be defined as

$$u(x,\theta,t)=U_{mn}^c\,sin(\lambda_m x)\,cos(\lambda_m x)\,cos(n\theta)$$
$$v(x,\theta,t)=V_{mn}^c\,sin^2(\lambda_m x)\,sin(n\theta) \tag{21}$$
$$w(x,\theta,t)=W_{mn}^c\,sin^2(\lambda_m x)\,cos(n\theta)$$
$$\phi(x,\theta,t)=\phi_{mn}^c\,sin^2(\lambda_m x)\,cos(n\theta)$$
$$\varphi(x,\theta,t)=\varphi_{mn}^c\,sin^2(\lambda_m x)\,cos(n\theta)$$

where, U_{mn}^c , V_{mn}^c , W_{mn}^c , ϕ_{mn}^c , φ_{mn}^c denote time-dependent unknown coefficients.

Substituting Eq. (21) into Eq. (16), produces

$$\begin{bmatrix}k_{11}^c & k_{12}^c & k_{13}^c & k_{14}^c & k_{15}^c\\ k_{21}^c & k_{22}^c & k_{23}^c & k_{24}^c & k_{25}^c\\ k_{31}^c & k_{32}^c & k_{33}^c & k_{34}^c & k_{35}^c\\ k_{41}^c & k_{42}^c & k_{43}^c & k_{44}^c & k_{45}^c\\ k_{51}^c & k_{52}^c & k_{53}^c & k_{54}^c & k_{55}^c\end{bmatrix}\cdot\begin{bmatrix}U_{mn}^c\\ V_{mn}^c\\ W_{mn}^c\\ \phi_{mn}^c\\ \varphi_{mn}^c\end{bmatrix}=\mathbf{0} \tag{22}$$

where,

$$k_{11}^c=-2(c_{11}h+2c_{11}^s)\lambda_m^2-(c_{66}h+2c_{66}^s)\frac{n^2}{2R^2}$$
$$k_{12}^c=-k_{21}^c=(c_{12}h+c_{66}h+2c_{12}^s+2c_{66}^s)\frac{n\lambda_m}{R}$$
$$k_{13}^c=-k_{31}^c=(c_{12}h+2c_{12}^s)\frac{\lambda_m}{R}$$
$$k_{14}^c=k_{15}^c=k_{51}^c=k_{41}^c=0$$
$$k_{22}^c=(c_{22}h+\frac{c_{22}h^3}{12R^2}+2c_{22}^s+\frac{c_{22}^s h^2}{2R^2})\frac{n^2}{2R^2}$$
$$+2(c_{66}h+\frac{c_{66}h^3}{12R^2}+2c_{66}^s+\frac{c_{66}^s h^2}{2R^2})\lambda_m^2$$
$$k_{23}^c=k_{32}^c=2\left(\frac{c_{12}h}{12}+\frac{c_{66}h}{6}+\frac{c_{12}^s}{2}+c_{66}^s\right)\frac{nh^2\lambda_m^2}{R^2}$$
$$+(\frac{c_{22}h}{6}+c_{22}^s)\frac{h^2n^3}{4R^4}+(c_{22}h+2c_{22}^s)\frac{n}{2R^2}$$
$$k_{24}^c=(\tilde{e}_{32}+he_{32}^s\eta)\frac{n}{2R^2}$$
$$k_{25}^c=(\tilde{f}_{32}+hf_{32}^s\eta)\frac{n}{2R^2}$$
$$k_{33}^c=(c_{22}h+2c_{22}^s)\frac{1}{2R^2}+4\left(\frac{c_{11}h}{6}+c_{11}^s\right)h^2\lambda_m^4$$
$$+2\left(\frac{c_{12}h}{6}+\frac{c_{66}h}{3}+c_{12}^s+2c_{66}^s\right)\frac{h^2n^2\lambda_m^2}{R^2}$$
$$+\left(\frac{c_{22}h}{6}+c_{22}^s\right)\frac{h^2n^4}{4R^4}+2\left(N_x^0+P-k_p-2\tau^s\right)\lambda_m^2$$
$$+(N_\theta^0-2\tau^s)\frac{n^2}{2R^2}-\frac{k_w}{2}$$
$$-(ea)^2[-2(N_x^0+P-k_p)(4\lambda_m^2+\frac{n^2}{R^2})\lambda_m^2$$
$$-\frac{n^2N_\theta^0}{R^2}(2\lambda_m^2+\frac{n^2}{2R^2})+2k_w\lambda_m^2+\frac{k_w n^2}{2R^2}]$$
$$k_{34}^c=2(\tilde{e}_{31}+e_{31}^s h\eta)\lambda_m^2+(\tilde{e}_{32}+e_{32}^s h\eta)\frac{n^2}{2R^2}$$
$$k_{35}^c=2(\tilde{f}_{31}+f_{31}^s h\eta)\lambda_m^2++(\tilde{f}_{32}+f_{32}^s h\eta)\frac{n^2}{2R^2}$$
$$k_{42}^c=-\frac{n\tilde{e}_{32}}{2R^2}-(ea)^2\frac{n\tilde{e}_{32}}{R^2}(2\lambda_m^2+\frac{n^2}{2R^2})$$

$$k_{43}^c = -(2\tilde{e}_{31}\lambda_m^2 + \frac{n^2\tilde{e}_{32}}{2R^2}) - (ea)^2[2\tilde{e}_{31}(4\lambda_m^2 + \frac{n^2}{R^2})\lambda_m^2 + \frac{n^2\tilde{e}_{32}}{R^2}(2\lambda_m^2 + \frac{n^2}{2R^2})]$$

$$k_{44}^c = 2\tilde{h}_{11}\lambda_m^2 + \tilde{h}_{22}\frac{n^2}{2} + l_g^2[2\tilde{h}_{11}\lambda_m^2(4\lambda_m^2 + \frac{n^2}{R^2}) + \tilde{h}_{22}n^2(2\lambda_m^2 + \frac{n^2}{2R^2})] + \frac{\tilde{h}_{33}}{2} + (ea)^2\tilde{h}_{33}(2\lambda_m^2 + \frac{n^2}{2R^2})$$

$$k_{45}^c = 2\tilde{g}_{11}\lambda_m^2 + \tilde{g}_{22}\frac{n^2}{2} + \frac{\tilde{g}_{33}}{2} + (ea)^2\tilde{g}_{33}(2\lambda_m^2 + \frac{n^2}{2R^2}) + l_g^2[2\tilde{g}_{11}\lambda_m^2(4\lambda_m^2 + \frac{n^2}{R^2}) + \tilde{g}_{22}n^2(2\lambda_m^2 + \frac{n^2}{2R^2})]$$

$$k_{52}^c = -\frac{n\tilde{f}_{32}}{2R^2} - (ea)^2\frac{n\tilde{f}_{32}}{R^2}(2\lambda_m^2 + \frac{n^2}{2R^2})$$

$$k_{53}^c = -(2\tilde{f}_{31}\lambda_m^2 + \frac{n^2\tilde{f}_{32}}{2R^2}) - (ea)^2[2\tilde{f}_{31}\lambda_m^2(4\lambda_m^2 + \frac{n^2}{R^2}) + \frac{n^2\tilde{f}_{32}}{R^2}(2\lambda_m^2 + \frac{n^2}{2R^2})]$$

$$k_{54}^c = 2\tilde{g}_{11}\lambda_m^2 + \tilde{g}_{22}\frac{n^2}{2} + \frac{\tilde{g}_{33}}{2} + (ea)^2\tilde{g}_{33}(2\lambda_m^2 + \frac{n^2}{2R^2}) + l_g^2[2\tilde{g}_{11}\lambda_m^2(4\lambda_m^2 + \frac{n^2}{R^2}) + \tilde{g}_{22}n^2(2\lambda_m^2 + \frac{n^2}{2R^2})]$$

$$k_{55}^c = 2\tilde{r}_{11}\lambda_m^2 + \tilde{r}_{22}\frac{n^2}{2} + \frac{\tilde{r}_{33}}{2} + (ea)^2\tilde{r}_{33}(2\lambda_m^2 + \frac{n^2}{2R^2}) + l_g^2[2\tilde{r}_{11}\lambda_m^2(4\lambda_m^2 + \frac{n^2}{R^2}) + \tilde{r}_{22}n^2(2\lambda_m^2 + \frac{n^2}{2R^2})]$$

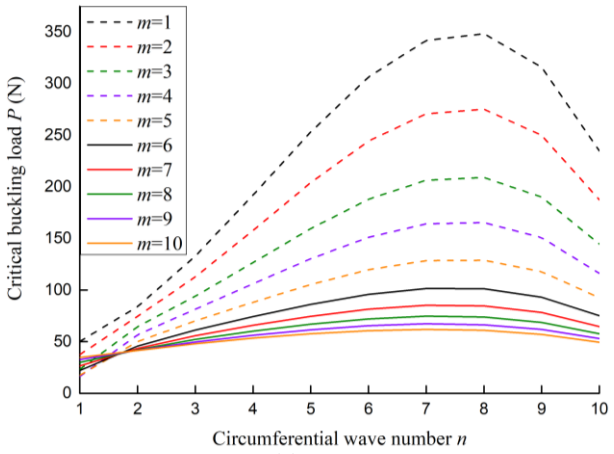

(a) S-S

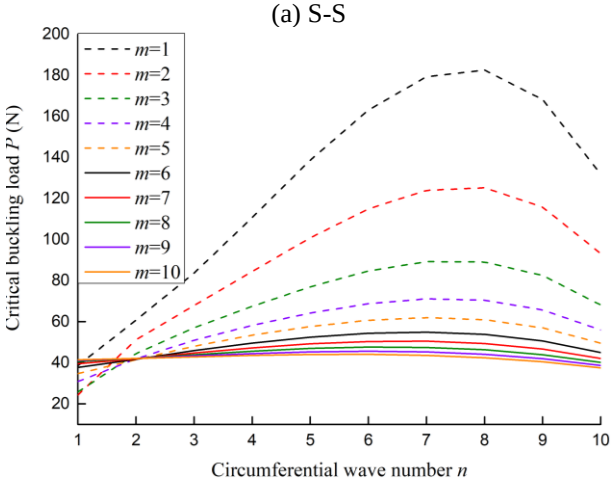

(b) C-C

Fig. 2 Effect of axial wave number m on critical buckling load P vs. the circumferential wave number n

4. Results and discussion

In this part, the numerical results are shown in Figs. 2-10 according to the bifurcation conditions gained in previous part. The effects of temperature change, initial electric potential, initial magnetic potential, scale parameters, Winkler and Pasternak coefficients, axial and circumferential wave numbers on the critical buckling load of a TEME cylindrical nano-shell under different edge conditions are investigated. The properties mentioned in Table 1 are employed, and the geometric parameters of the nano-shell are L = 200nm, R = 20nm, h = 1nm. The units of the Winkler and Pasternak coefficients are N/m^3 and N/m, respectively.

Fig. 2 demonstrates the effects of axial and circumferential wave numbers on the critical buckling load of TEME cylindrical nano-shells with S-S edges and C-C edges, respectively. As can be seen, critical buckling load increases to its maximum value by increasing circumferential wave number to 8, and then decreases, for both two edge conditions. In this circumstance (ea =1nm, l_g=1nm, τ^s = 1N/m, k_w= 10^{-2} N/m^3, k_p = 10^{-4} N/m, ΔT = 300K, ϕ_0 = -0.4V, φ_0 = -0.0002A), the maximum critical buckling load occurs at the 8th order of circumferential number, i.e., the most difficult circumferential buckling for the shell (maximum circumferential number) is n = 8. In addition, it can be realized that an increase of axial wave number, leads to decrease in critical buckling load in both two kinds of edge conditions, which indicates that the increase of axial wave number tends to decrease the buckling behavior of the shell. Furthermore, the larger the axial wave number is, the smaller the intervals between the curves of critical buckling load will be, indicating that the shell is susceptible to order jump when higher-order axial buckling occurs. Moreover, from comparing of the results corresponding to S-S and C-C nano-shells, showing that, critical buckling load of the shell with S-S edges is higher than that with C-C edges. It can be concluded that the TEME cylindrical nano-shell exhibits more increased stiffness with S-S edges than with C-C edges.

Figs. 3-5 display the influences of scale parameters on the critical buckling load of a TEME cylindrical nano-shell. It also can be found that the critical buckling load of S-S nano-shells is larger than the C-C nano-shells.

It can be concluded from Fig. 3 that, the critical buckling load first sharply decreases with the increase of axial wave number, and then slowly decreases to a stable value in both two kinds of edge conditions. It is interesting to note that, the lower the value of the axial wave number (m<4), the greater the impact of the axial wave number on critical buckling load. However, the difference is diminishing as axial wave number becomes large. It also can be witnessed

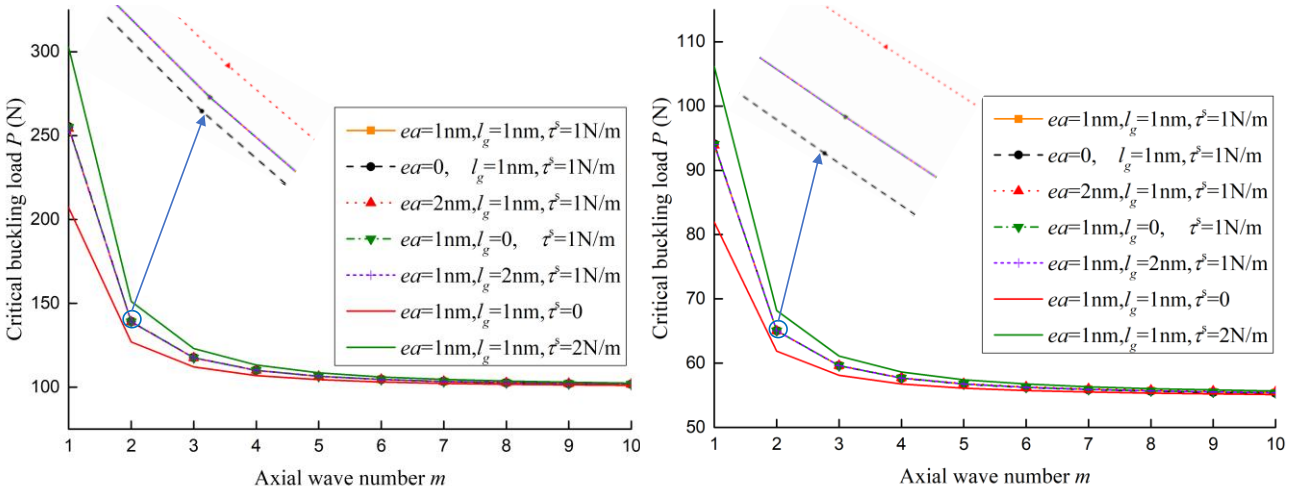

(a) S-S (b) C-C

Fig. 3 Variations of critical buckling load P for several values of nonlocal parameter ea, strain gradient parameter l_g and residual surface stress τ^s versus the axial wave number m $(n = 5)$

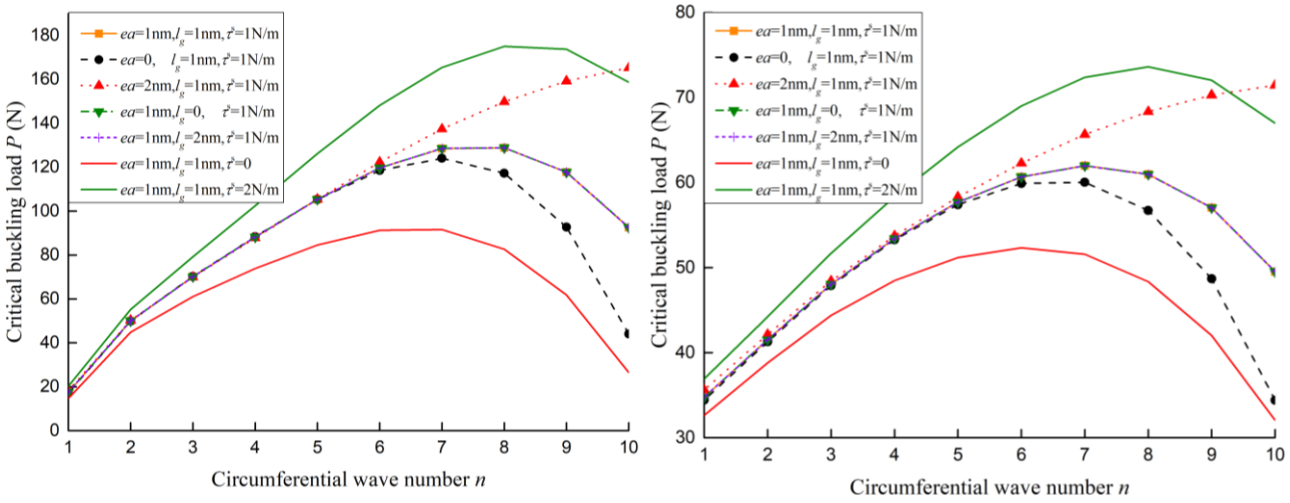

(a) S-S (b) C-C

Fig. 4 Variations of critical buckling load P for several values of nonlocal parameter ea, strain gradient parameter l_g and residual surface stress τ^s versus the circumferential wave number n $(m = 5)$

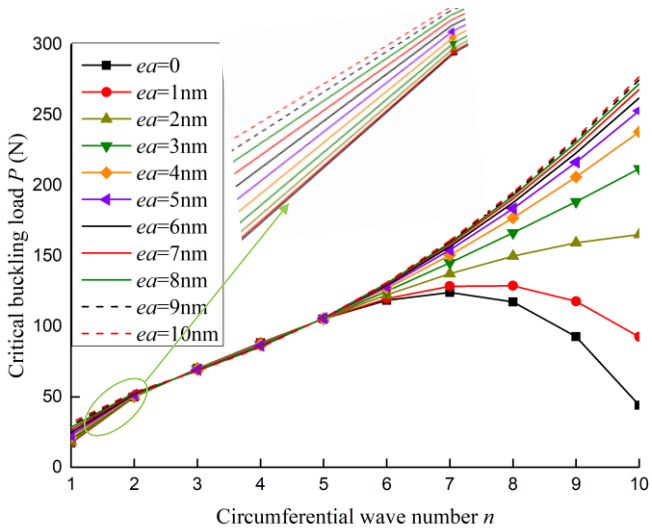

Fig. 5 Effect of nonlocal parameter on critical buckling load versus the circumferential wave number $(m = 5)$ with S-S edges

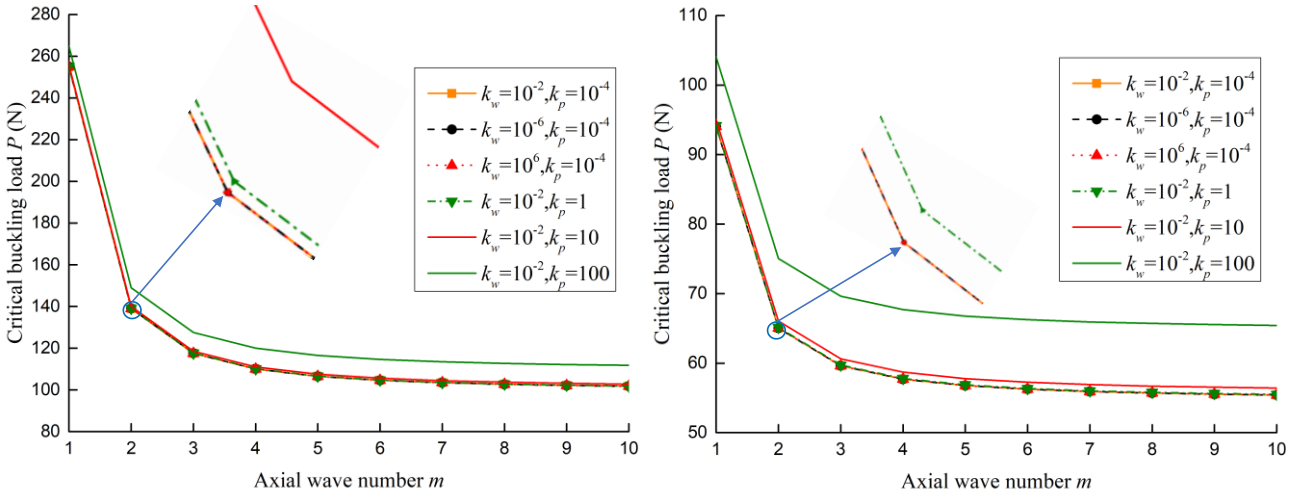

(a) S-S (b) C-C

Fig. 6 Variations of critical buckling load P for several values of Winkler coefficient k_w and Pasternak coefficient k_p versus the axial wave number m $(n = 5)$

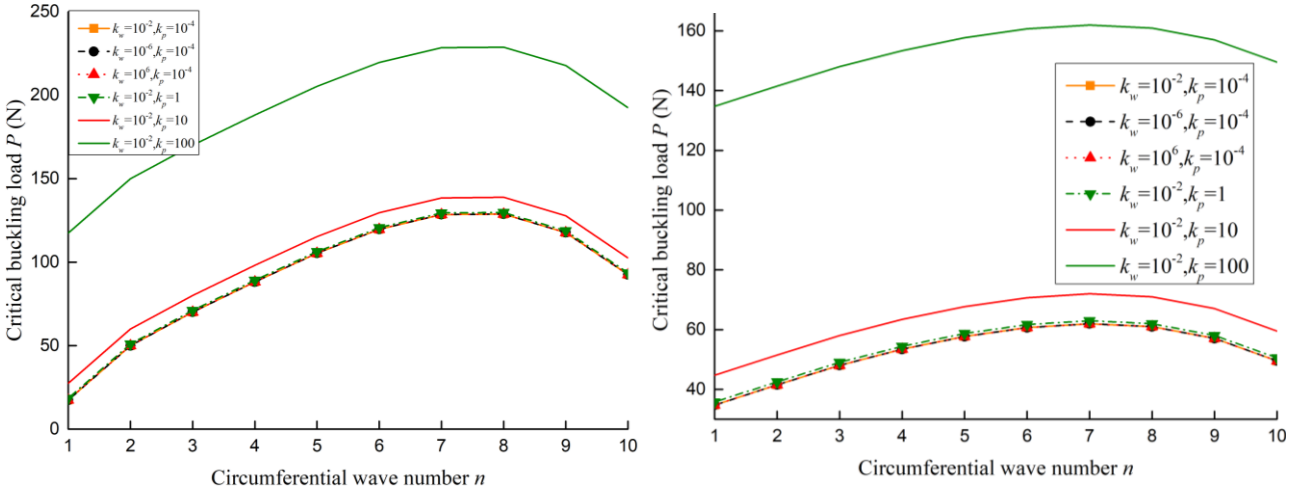

(a) S-S (b) C-C

Fig. 7 Variations of critical buckling load P for several values of Winkler coefficient k_w and Pasternak coefficient k_p versus the circumferential wave number n $(m = 5)$

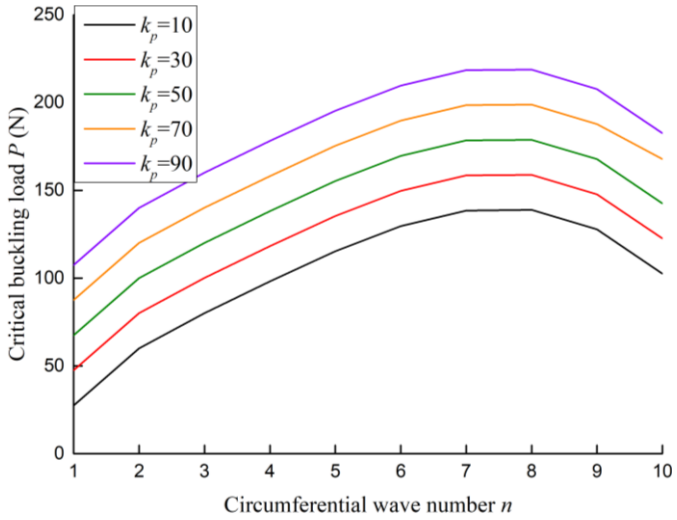

Fig. 8 Effect of Pasternak coefficient on critical buckling load versus the circumferential wave number $(m = 5)$ with S-S edges

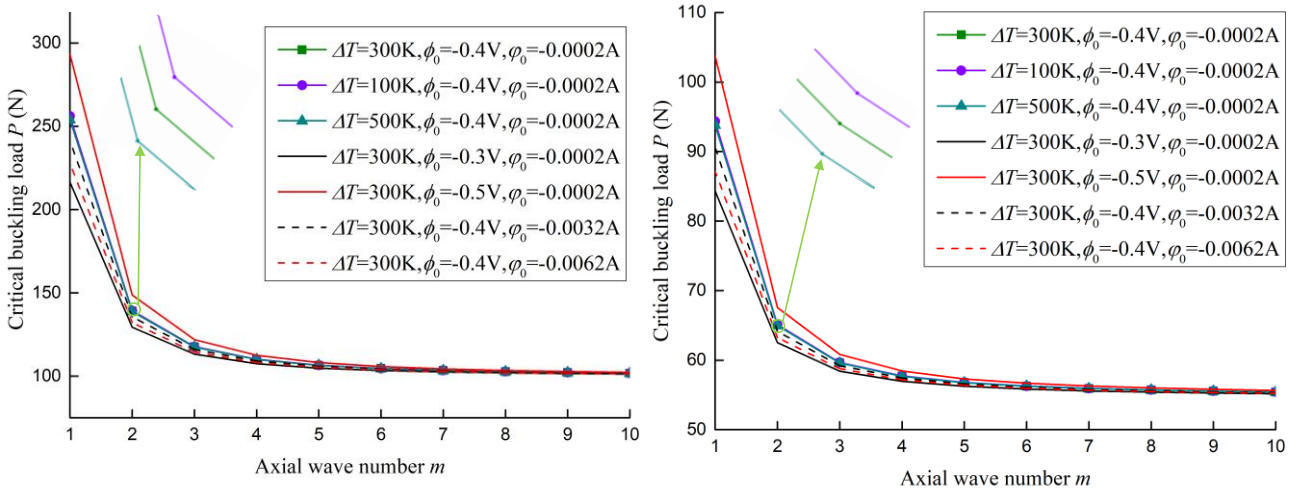

(a) S-S (b) C-C

Fig. 9 Variations of critical buckling load P for several values of temperature change ΔT, initial electric potential ϕ_0 and initial magnetic potential φ_0 versus the axial wave number ($n = 5$)

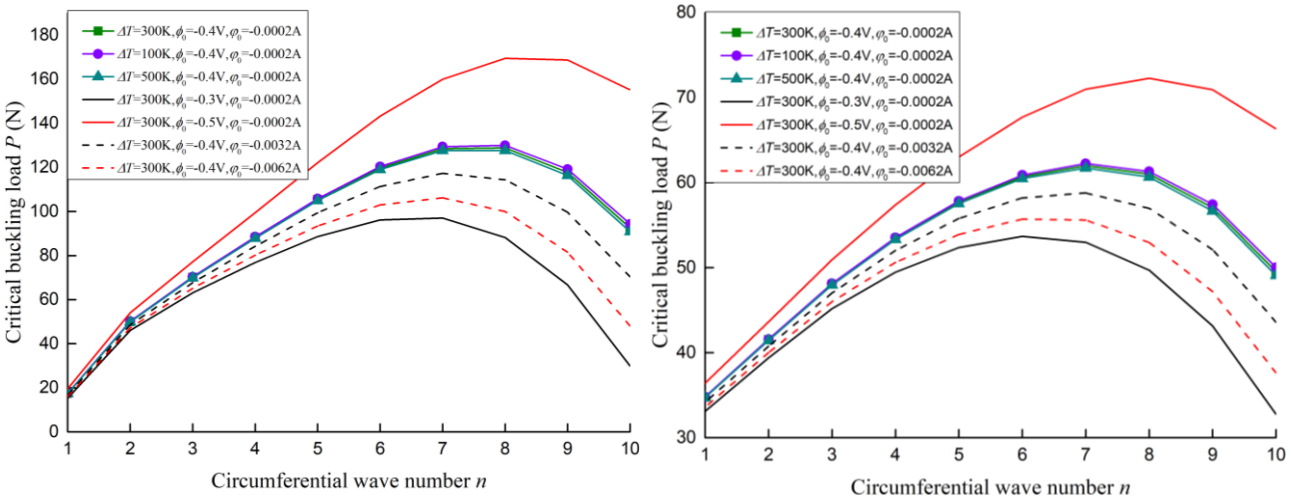

(a) S-S (b) C-C

Fig. 10 Variations of critical buckling load P for several values of temperature change ΔT, initial electric potential ϕ_0 and initial magnetic potential φ_0 versus the circumferential wave number ($m = 5$)

that the curves of the critical buckling load versus axial wave number can be raised by applying greater residual surface stress or nonlocal parameter. Nevertheless, the influence of strain gradient parameter on the critical buckling load is inconspicuous. It can be said that the residual surface stress has the greatest impact on the critical buckling load among the scale parameters.

As it can be seen from Fig. 4, the curves of critical buckling load versus circumferential wave number elevate as the residual surface stress is increased for two types of edge conditions. The curves of critical buckling load corresponding to different nonlocal parameters are overlapping for the values n<6. In other words, nonlocal parameter has little effect on critical buckling load on the first 5 circumferential orders. It is noteworthy that, the change in nonlocal parameter can change the value of the circumferential wave number corresponding to the highest point of the curves, for the values n>6. In other words, change in nonlocal parameter could change the maximum circumferential number. For S-S and C-C nano-shells in which the influence of strain gradient effect on critical buckling load is negligible.

Fig. 5 could further study the nonlocal effect, the numerical values display that the larger the nonlocal parameter is, the higher the curve of critical buckling load will be. This also indicates that the nonlocal effect is significant for the higher-order circumferential buckling of the TEME nano-shells.

Figs. 6-8 reveal the influences of Winkler and Pasternak coefficients on the critical buckling load of a TEME cylindrical nano-shell.

It is concluded from Figs. 6 and 7 that, when the Pasternak coefficient is larger and larger, the curves of the critical buckling load are higher and higher. This means that Pasternak foundation intensifies the stiffness of the nano-shell. Moreover, the effect of Pasternak foundation on the critical buckling load is more considerable compared to the effect of the Winkler foundation.

It is noteworthy from Fig. 8 that the change in Pasternak coefficient will not change the circumferential wave number corresponding to the highest point of the critical buckling load curves, i.e., Pasternak coefficient will not change the maximum circumferential number.

Figs. 9 and 10 illustrate the influences of temperature change, initial electric and magnetic potentials on the critical buckling load of a TEME cylindrical nano-shell with S-S edges and C-C edges. As can be seen, critical buckling load of the shell with S-S edges is always higher than that with C-C edges.

As illustrated in Fig. 9, it can be seen that an increase in the negative value of initial electric potential leads to increasing the critical buckling load. It can be deduced that an increase in the negative voltage leads to increasing the critical buckling load and consequently increasing the stiffness-hardening behavior. Conversely, increasing the negative initial magnetic potential results in decreasing the critical buckling load. This means that the stiffness-hardening behavior of TEME nano-shells decreases via an increase in the negative initial magnetic potential. Additionally, an increase in temperature change leads to decreasing the critical buckling load, this is due to the fact that rising the temperature change would decrease in stiffness of the nano-shells. And this effect is very small and insignificant in comparison with those of electric voltage and magnetic potential. Moreover, the curves of critical buckling load tend to converge as the axial wave number increases. It means that variation of initial electric and magnetic environments cannot affect the critical buckling load of the shell when the axial wave number is large.

Fig. 10 illustrates that change in initial electric potential or magnetic potential will change the maximum circumferential number, while temperature change has no effect on the maximum circumferential number. In addition, the curves of critical buckling load tend to converge as the circumferential wave number decreases, it means that variation of temperature change, initial electric or magnetic environment has little effect on the critical buckling load of the shell when the circumferential wave number is small.

5. Conclusions

An analytical Hamiltonian-based method is applied into the buckling of an embedded TEME cylindrical nano-shell. The Winkler and Pasternak elastic foundations as well as thermo-electro-magneto-mechanical loadings are applied, and two different types of edge conditions (S-S edges and C-C edges) are taken into the investigation. The novel scale-dependent model presents the multi-field coupling and nanostructure effects exhibited by the TEME cylindrical shell at nano scale. Some useful conclusions can be summarized as follows:

• The TEME cylindrical nano-shell exhibits more increased stiffness with S-S edges than with C-C edges.

• The increase of axial wave number tends to decrease the buckling behavior of the nano-shell. And the nano-shell is susceptible to order jump when higher-order axial buckling occurs.

• The residual surface stress has the greatest impact on the critical buckling load among the scale parameters, while the influence of strain gradient effect is negligible. The nonlocal effect is significant for the higher-order circumferential buckling of the nano-shell. In addition, change in nonlocal parameter could change the maximum circumferential number.

• Pasternak foundation intensifies the stiffness of the nano-shell, and the effect of Pasternak foundation on the critical buckling load is more considerable compared to the effect of the Winkler foundation.

• Variation of initial electric and magnetic environments cannot affect the critical buckling load of the nano-shell when the axial wave number is large. Variation of temperature change, initial electric or magnetic environment has little effect on the critical buckling load of the nano-shell when the circumferential wave number is small. Moreover, change in initial electric potential or magnetic potential will also change the maximum circumferential number.

References

Arefi, M., Kiani, M. and Zamani, M.H. (2020), "Nonlocal strain gradient theory for the magneto-electro-elastic vibration response of a porous FG-core sandwich nanoplate with piezomagnetic face sheets resting on an elastic foundation", *J. Sandw. Struct. Mater.*, **22**, 2157-2185. https://doi.org/10.1177/1099636218795378.

Boyina, K. and Piska, R. (2023), "Wave propagation analysis in viscoelastic Timoshenko nanobeams under surface and magnetic field effects based on nonlocal strain gradient theory", *Appl. Math. Comput.*, **439**, 127580. https://doi.org/10.1016/j.amc.2022.127580.

Dai, H.M. and Safarpour, H. (2021), "Frequency and thermal buckling information of laminated composite doubly curved open nanoshell", *Adv. Nano Res.*, **10**(1), 1-14. https://doi.org/10.12989/anr.2021.10.1.001.

Daikh, A.A., Houari, M.S.A. and Eltaher, M.A. (2021), "A novel nonlocal strain gradient Quasi-3D bending analysis of sigmoid functionally graded sandwich nanoplates", *Compos. Struct.*, **262**, 113347. https://doi.org/10.1016/j.compstruct.2020.113347.

Farzad, E. and Parisa, H. (2017), "Wave propagation analysis of rotating thermoelastically-actuated nanobeams based on nonlocal strain gradient theory", *Acta Mechanica Solida Sinica*, **30**, 647-657. https://doi.org/10.1016/j.camss.2017.09.007.

Frankland, S.J.V., Caglar, A., Brenner, D.W. and Griebel, M. (2002), "Molecular simulation of the influence of chemical cross-links on the shear strength of carbon nanotube polymer interfaces", *J. Phys. Chem. B*, **106**, 3046-3048. https://doi.org/10.1021/jp015591+.

Fraternali, F. and Paulino, G.H. (2020), "Mechanics research communications special issue on advances in mechanical metamaterials and smart structures", *Mech. Res. Commun.*, **107**, 103531. https://doi.org/10.1016/j.mechrescom.2020.103531.

Ghorbani, K., Rajabpour, A., Ghadiri, M. and Keshtkar, Z. (2020), "Investigation of surface effects on the natural frequency of a functionally graded cylindrical nanoshell based on nonlocal strain gradient theory", *Eur. Phys. J. Plus*, **135**, 701. https://doi.org/10.1140/epjp/s13360-020-00712-1.

Ghorbanpour, A.A., Abdollahian, M., Kolahchi, R. and Rahmati, A.H. (2013), "Electro-thermo-torsional buckling of an embedded armchair DWBNNT using nonlocal shear deformable shell model", *Compos. Part B Eng.*, **51**, 291-299.

https://doi.org/10.1016/j.compositesb.2013.03.017.
Gui, Y.F. and Li, Z.S. (2023), "A nonlocal strain gradient shell model with surface effect for buckling analysis of magneto-electro-thermo-elastic cylindrical nanoshell subjected to axial load", *Phys. Chem. Chem. Phys.*, **25**, 24838-24852. https://doi.org/10.1039/D3CP02880A.
Gui, Y.F. and Wu, R.J. (2023), "Buckling analysis of embedded thermo-magneto-electro-elastic nano cylindrical shell subjected to axial load with nonlocal strain gradient theory", *Mech. Res. Commun.*, **128**, 104043. https://doi.org/10.1016/j.mechrescom.2023.104043.
Hamidi, B.A., Hosseini, S.A. and Hayati, H. (2022), "Forced torsional vibration of nanobeam via nonlocal strain gradient theory and surface energy effects under moving harmonic torque", *Waves Random Complex Med.*, **32**, 318-333. https://doi.org/10.1080/17455030.2020.1772523.
Hosseini, S.M.J., Torabi, J., Ansari, R. and Zabihi, A. (2021), "Geometrically nonlinear electromechanical instability of FG nanobeams by nonlocal strain gradient theory", *Int. J. Struct. Stabil. Dyn.*, **21**, 2150051. https://doi.org/10.1142/S0219455421500516.
Huang, Y.Z., Feng, M.L. and Chen, X.H. (2022), "Pull-in instability and vibration of quasicrystal circular nanoplate actuator based on surface effect and nonlocal elastic theory", *Arch. Appl. Mech.*, **92**, 853-866. https://doi.org/10.1007/s00419-021-02077-y.
Jamalpoor, A., Ahmadi-Savadkoohi, A., Hosseini, M. and Hosseini-Hashemi, S. (2017), "Free vibration and biaxial buckling analysis of double magneto-electro-elastic nanoplate-systems coupled by a visco-Pasternak medium via nonlocal elasticity theory", *Eur. J. Mech. A Solids*, **63**, 84-98. https://doi.org/10.1016/j.euromechsol.2016.12.002.
Jena, S.K., Chakraverty, S. and Tornabene, F. (2019), "Dynamical behavior of nanobeam embedded in constant, linear, parabolic, and sinusoidal types of Winkler elastic foundation using first-order nonlocal strain gradient model", *Mater. Res. Exp.*, **6**, 850. https://doi.org/10.1088/2053-1591/ab2779.
Karimi, M. and Farajpour, M.R. (2019), "Bending and buckling analyses of $BiTiO_3$-$CoFe_2O_4$ nanoplates based on nonlocal strain gradient and modified couple stress hypotheses: rate of surface layers variations", *Appl. Phys.*, **125**, 530.1-530.16. https://doi.org/10.1007/s00339-019-2811-6.
Karimi, M. and Rafieian, S. (2019), "A comprehensive investigation into the impact of nonlocal strain gradient and modified couple stress models on the rates of surface energy layers of $BiTiO_3$-$CoFe_2O_4$ nanoplates: A vibration analysis", *Mater. Res. Exp.*, **6**, 075038. https://doi.org/10.1088/2053-1591/ab151b.
Ke, L.L., Wang, Y.S., Yang, J. and Kitipornchai, S. (2014), "The size-dependent vibration of embedded magneto-electro-elastic cylindrical nanoshells", *Smart Materi. Struct.*, **23**, 125036. https://doi.org/10.1088/0964-1726/23/12/125036.
Li, Z.W., Chen, B., Lin, B.C., Zhao, X. and Li, Y.H. (2022), "Analytical solutions of the forced vibration of Timoshenko micro/nano-beam under axial tensions supported on Winkler-Pasternak foundation", *Eur. Phys. J. Plus*, **137**, 153. https://doi.org/10.1140/epjp/s13360-022-02360-z.
Liew, K.M., He, X.Q. and Wong, C.H. (2004), "On the study of elastic and plastic properties of multi-walled carbon nanotubes under axial tension using molecular dynamics simulation", *Acta Materialia*, **52**, 2521-2527. https://doi.org/10.1016/j.actamat.2004.01.043.
Lu, L., Zhu, L., Guo, X.M., Zhao, J.Z. and Liu, G.Z. (2019), "A nonlocal strain gradient shell model incorporating surface effects for vibration analysis of functionally graded cylindrical nanoshells", *Appl. Math. Mech.*, **40**, 1695-1722. https://doi.org/10.1007/s10483-019-2549-7.
Mamandi, A. (2023), "Nonlocal large deflection analysis of a cantilever nanobeam on a nonlinear Winkler-Pasternak elastic foundation and under uniformly distributed lateral load", *J. Mech. Sci. Technol.*, **37**, 813-824. https://doi.org/10.1007/s12206-023-0124-3.
Moaaz, O., Abouelregal, A.E. and Alsharari, F. (2022), "Lateral vibration of an axially moving thermoelastic nanobeam subjected to an external transverse excitation", *AIMS Math.*, **8**, 2272-2295. 10.3934/math.2023118.
Momeni-Khabisi, H. and Tahani, M. (2022), "A size-dependent study on buckling and post-buckling behavior of imperfect piezo-flexomagnetic nano-plate strips", *Adv. Nano Res.*, **12**(4), 427-440. https://doi.org/10.12989/anr.2022.12.4.427.
Ni, Y.W., Zhu, S.B., Sun, J.B., Tong, Z.Z., Zhou, Z.H. and Xu, X.S. (2020), "Analytical buckling solution of magneto-electro-thermo-elastic cylindrical shells under multi-physics fields", *Compos. Struct.*, **239**, 112021. https://doi.org/10.1016/j.compstruct.2020.112021.
Nicolae, H., Bogdan, M. and Vasile, M. (2022), "Nonlinear vibration of double-walled carbon nanotubes subjected to mechanical impact and embedded on Winkler-Pasternak foundation", *Materials*, **15**, 8599. https://doi.org/10.3390/ma15238599.
Pham, Q., Nguyen, P., Tran, V.K., Lieu, Q.X. and Tran, T.T. (2023), "Modified nonlocal couple stress isogeometric approach for bending and free vibration analysis of functionally graded nanoplates", *Eng. Comput.*, **39**, 993-1018. https://doi.org/10.1007/s00366-022-01726-2.
Qu, Y.L., Pan, E., Zhu, F., Jin, F. and Roy, A.K. (2023), "Modeling thermoelectric effects in piezoelectric semiconductors: New fully coupled mechanisms for mechanically manipulated heat flux and refrigeration", *Int. J. Eng. Sci.*, **182**, 103775. https://doi.org/10.1016/j.ijengsci.2022.103775.
Timesli, A. (2020), "Buckling analysis of double walled carbon nanotubes embedded in Kerr elastic medium under axial compression using the nonlocal Donnell shell theory", *Adv. Nano Res.*, **9**(2), 69-82. https://doi.org/10.12989/anr.2020.9.2.069.
Timesli, A. (2021), "A cylindrical shell model for nonlocal buckling behavior of CNTs embedded in an elastic foundation under the simultaneous effects of magnetic field, temperature change, and number of walls", *Adv. Nano Res.*, **11**(6), 581-593. https://doi.org/10.12989/anr.2021.11.6.581.
Tiwari, R., Abouelregal, A.E., Shivay, O.N. and Megahid, S.F. (2022), "Thermoelastic vibrations in electro-mechanical resonators based on rotating microbeams exposed to laser heat under generalized thermoelasticity with three relaxation times", *Mech. Time Depend. Mater.*, 1-25. https://doi.org/10.1007/s11043-022-09578-5.
Tran, M.T., Nguyen, V.L., Pham, S. and Rungamornrat, J. (2020), "Free vibration of stiffened functionally graded circular cylindrical shell resting on Winkler-Pasternak foundation with different boundary conditions under thermal environment", *Acta Mech.*, **231**, 2545-2564. https://doi.org/10.1007/s00707-020-02658-y.
Wang, X. and Jin, F. (2022), "Shear horizontal wave propagation in multilayered magneto-electro-elastic nanoplates with consideration of surface/interface effects and nonlocal effects", *Waves Random Complex Med.*, 1-20. https://doi.org/10.1080/17455030.2022.2134599.
Wang, Y., Feng, C., Zhao, Z., Lu, F.Z. and Yang, J. (2018a), "Torsional buckling of graphene platelets (GPLs) reinforced functionally graded cylindrical shell with cutout", *Compos. Struct.*, **197**, 72-79. https://doi.org/10.1016/j.compstruct.2018.05.056.
Wang, Y., Feng, C., Zhao, Z. and Yang, J. (2018b), "Buckling of graphene platelet reinforced composite cylindrical shell with

cutout", *Int. J. Struct. Stabil. Dyn*., **18**, 1850040. https://doi.org/10.1142/S0219455418500402.

Wang, Y., Feng, C., Zhao, Z. and Yang, J. (2018c), "Eigenvalue buckling of functionally graded cylindrical shells reinforced with graphene platelets (GPL)", *Compos. Struct*., **202**, 38-46. https://doi.org/10.1016/j.compstruct.2017.10.005.

Zeighampour, H., Beni, Y.T. and Kiani, Y. (2020), "Electric field effects on buckling analysis of Boron-Nitride nanotubes using surface elasticity theory", *Int. J. Struct. Stabil. Dyn*., **20**, 2050137. https://doi.org/10.1142/S0219455420501370.

Zhang, G.Y., Gao, X.L. and Littlefield, A.G. (2021), "A non-classical model for circular cylindrical thin shells incorporating microstructure and surface energy effects", *Acta Mechanica*, **232**, 2225-2248. https://doi.org/10.1007/s00707-020-02873-7.

Zhang, G.Y., Qu, Y.L., Gao, X.L. and Jin, F. (2020), "A transversely isotropic magneto-electro-elastic Timoshenko beam model incorporating microstructure and foundation effects", *Mech. Mater*., **149**, 103412. https://doi.org/10.1016/j.mechmat.2020.103412.

Zur, K.K., Arefi, M., Kim, J. and Reddy, J.N. (2020), "Free vibration and buckling analyses of magneto-electro-elastic FGM nanoplates based on nonlocal modified higher-order sinusoidal shear deformation theory", *Compos. Part B, Eng*., **182**, 107601. https://doi.org/10.1016/j.compositesb.2019.107601.

CC